

Department of Mechanical and Aerospace Engineering

ME-UY 4214 Finite Element Modeling, Design, and Analysis

Spring 2025



Final Report: Drone Frame Analysis

Group: 2

MEMBER NAME	MEMBER ID	Contributions
Radhika Mishra	rm6326	Conclusion, Fluent Analysis, Calculations
Sarah Lenzi	sml9655	Introduction, Model, Thermal Analysis, CAD Model
Shristhi Pant	sp7171	Modal Analysis, Discussion
Tahasin Iqbal	tji8225	CAD Model, Static Structural Analysis, Calculations

Table of Contents

1. Introduction.....	3
2. Model.....	4
3. Results.....	6
3.1. Static Structural Analysis.....	6
3.2. Steady-State Thermal Analysis.....	16
3.3. Modal Analysis.....	20
3.4. Fluent Analysis.....	26
4. Discussion.....	33
5. Conclusion.....	36
7. References.....	38

1. Introduction

Drones are a widely used application in industries, in everything from surveillance and rescue operations to delivery and photography. The objective of analyzing the drone frame is to determine the structural integrity under various loading and force conditions. The frame undergoes different levels of deformation, stress, and strain from different forces, including aerodynamic forces, landing impact, and weight distribution of the onboard components (ie, batteries, wires, etc.).

It is vital to remember that when designing a drone frame, there is stability and balance in the structure. This is an engineering problem that can be analyzed under a microscope, or in this case, using Finite Element Modeling, Design, and Analysis methods. A poorly designed frame can lead to mechanical failure, excessive vibrations, or inefficient flight performance. Ensuring structural stability of the framing can help reach code safety regulations, proper performance, and efficiency. The goal is to optimize the drone frame structure integrity and thermal stability by ensuring it meets strength and deflection criteria and design requirements.

The geometry model that will be analyzed is equated to a quadcopter frame, one commonly used that has four arms extending symmetrically from the center to support the motors. The model will include key components such as the central hub, mounts, and reinforcements.

Drone technology is rapidly advancing, and structural reliability is a major concern for manufacturers and users. Applying finite element analysis (FEA) to study the structural behavior of a drone frame will allow for a detailed evaluation of potential failing points and optimization

of the materials and geometry used. The plan to analyze the frame includes conducting multiple simulation cases, including: Static Structural, Steady-State Thermal, Modal, and Fluent Analysis. Each of these simulations will show how the frame handles forces, temperatures, gravity, acceleration, and more real-world applications. The way the frame ‘reacts’ will give insight to design improvements to create more durability, efficiency, and safety.

2. Model

The frame under analysis can be seen in Figure 1. It is an assembly made from two legs, four arms, eight pins, one body, and four blades. The body of this drone, made from wrought grade aluminum, is created to emulate where a standard drone would hold batteries, and it is pinned to the arms with steel pins. The propeller blades, made from aluminum, are pinned to the end of each of the four arms using more steel pins. The legs, created for the drone landing and to absorb the impact of a landing, are created from the same aluminum as the body, arms, and blades. The material of the frame is Aluminum Alloy, Wrought, 6061, because of its lightweight and strong material. The details of each of the materials can be found below in Table 1.

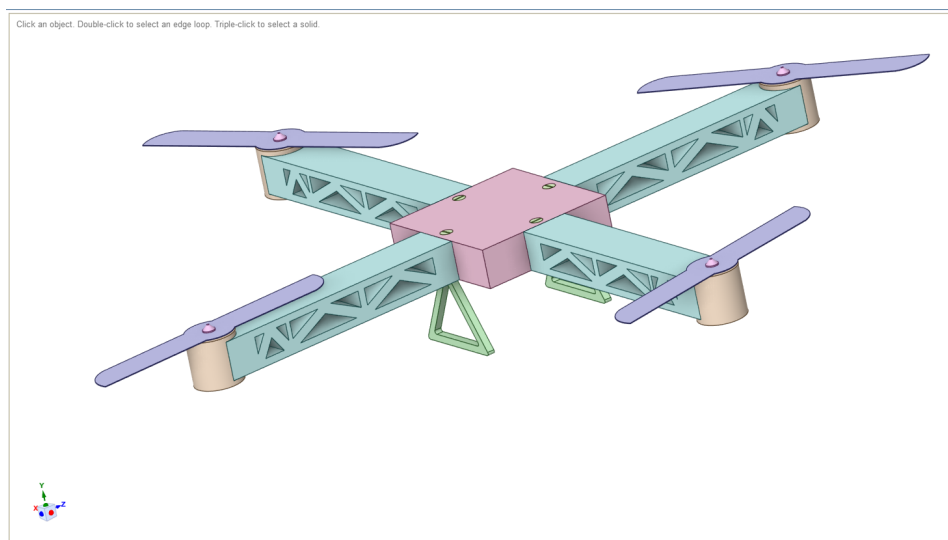


Figure 1: Geometry of Drone Frame

The frame was modeled using Aluminum Alloy 6061-T6, a widely used aerospace-grade alloy selected due to the following advantages:

- High strength-to-weight ratio
- Corrosion resistance
- Good machinability and weldability
- Proven use in UAV and aerospace frames

Table 1: Materials of the Drone Parts

Parts	Quantity	Materials	Young's Modulus (Pa)	Poisson's Ratio	Tensile Yield Strength (23 C)
Legs	2	Aluminium Alloy, Wrought, 6061, T6	6.904E+10	0.33	2.592E+08
Arms	4	Aluminium Alloy, Wrought, 6061, T6	6.904E+10	0.33	2.592E+08
Pins	8	316 Stainless Steel	2E+11	0.3	2.744E+07
Body	1	Aluminium Alloy, Wrought, 6061, T6	6.904E+10	0.33	2.592E+08
Blades	4	Aluminium Alloy, Wrought, 6061, T6	6.904E+10	0.33	2.592E+08

A fine mesh resolution of 0.02 mm was applied to ensure high accuracy in detecting deformation and stress gradients, especially in regions with high geometric complexity and load application.

The general mesh setup of the model was set to a tetrahedral shape and a resolution of 4 to ensure a finer mesh detail and more accuracy when analyzing the results (Figure 2).

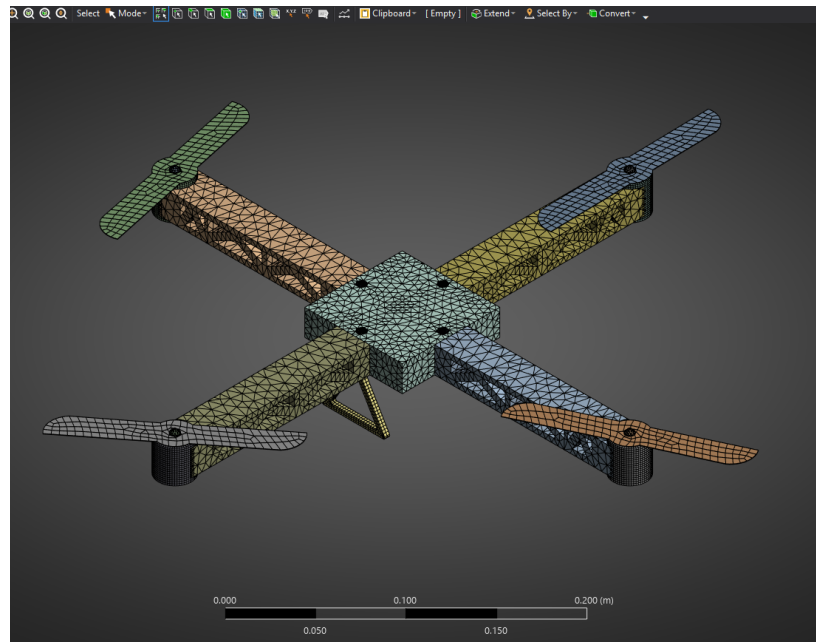


Figure 2: Basic Generated Mesh of the Frame

3. Results

3.1. Static Structural Analysis

The Static Structural analysis aims to evaluate the structural integrity of a quadcopter drone frame under two critical load conditions: takeoff and landing. It will use static structural simulation in ANSYS to determine maximum stress, total deformation, and assess the safety factor of the frame to ensure it operates safely during these stages of flight.

3.1. a. CASE A: Thrust for Takeoff

Design Assumptions and Load Justification:

The drone mass is obtained using the Solidworks Mass Properties Section. Drone Mass,

$$m = 0.82 \text{ lb} = 0.372 \text{ kg}$$

$$\text{Gravitational acceleration, } g = 9.8 \text{ m/s}^2$$

$$\text{Drone Weight, } W = mg = 3.65 \text{ N}$$

Typically, drones are designed to generate at least 1.5 to 2 times their weight in thrust to ensure adequate lifting capacity and provide sufficient maneuverability (Average Drone Thrust Data).

Now, the calculations assume that the thrust weight of landing is 2 times their weight. This factor includes a safety margin to account for air resistance, maneuvering forces, and dynamic conditions. So, to safely lift off, the Total required thrust,

$$T_{thrust} = 2 * 3.65 \text{ N} = 7.3 \text{ N}$$

Per Propellers (4 arms):

Force per motor mount,

$$F_{thrust \text{ per arm}} = \frac{7.3 \text{ N}}{4} = 1.825 \text{ N}$$

Applied thrust force on the bottom face of each motor mount cylinder (upward Y-direction).

The frame of the quadcopter is analyzed to test its feasibility, rigidity, and compatibility. It consists of static analysis. The rigidity of the quadcopter body frame was analyzed considering

the equality between the vertical thrust produced by each motor and the weight of the quadcopter during the flight time.

The boundary conditions for takeoff are provided below:

Boundary Conditions for Takeoff:

Supports (Fixed Constraints):

- The bottom face of the landing legs was fully constrained (fixed support), simulating the drone on the ground before lift-off.

Applied Loads:

- A vertical upward force of 1.825 N was applied on the top face of each motor mount (not the bottom), accurately simulating the thrust generated by motors pushing the frame upward during takeoff.

Purpose of Setup:

- This configuration realistically mimics the physical reaction force of thrust applied by the motors, which are mounted on top and generate an upward force to lift the drone.

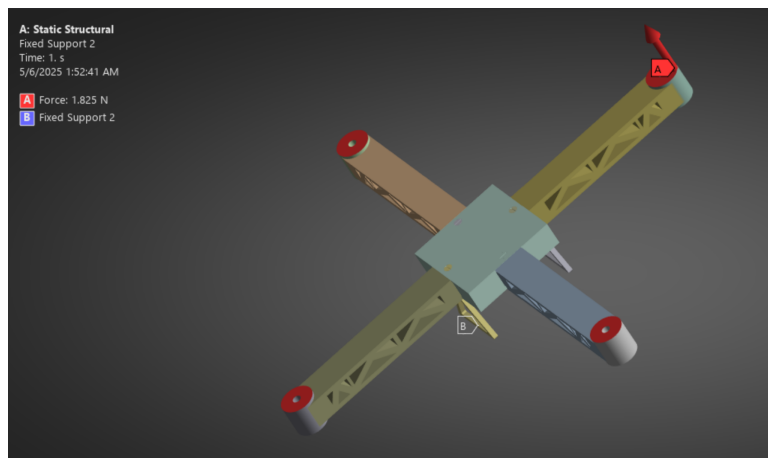


Figure 3: Takeoff Boundary Conditions

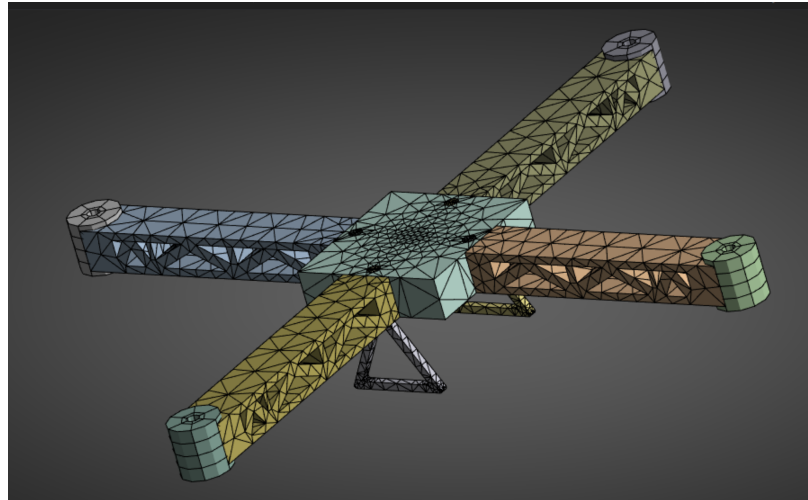


Figure 4: Generated Mesh

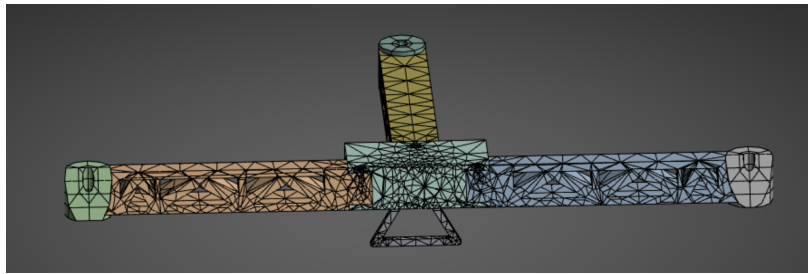


Figure 5: Cross-Section View of Mesh

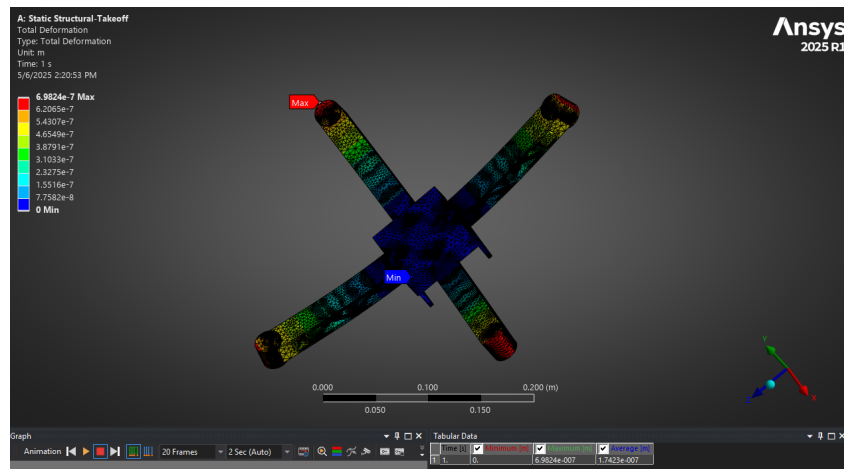


Figure 6: Total Deformation of the Drone

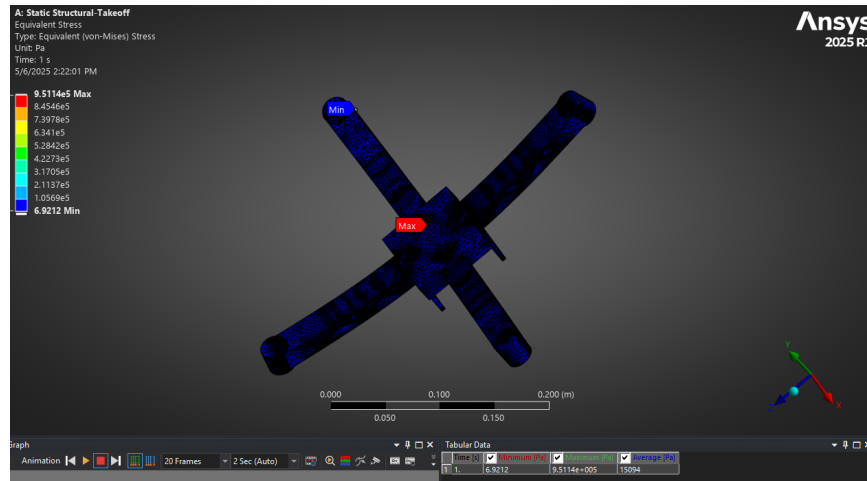


Figure 7: Equivalent (Von-Mises) Stress

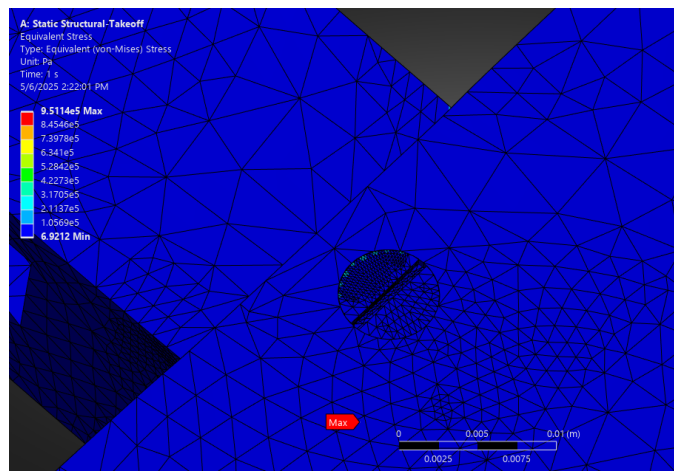


Figure 8: Close-Up View of Maximum Stress

Table 2: Average Stress

Times [s]	Minimum [Pa]	Maximum [Pa]	Average [Pa]
1.	6.9212	9.5114E+005	15094

Based on Table 2, the maximum stress observed during takeoff is approximately 951 KPa, significantly below the tensile strength of Aluminium Wrought 6061-T6 (approximately 259 MPa).

The safety factor of drones is also analyzed in ANSYS.

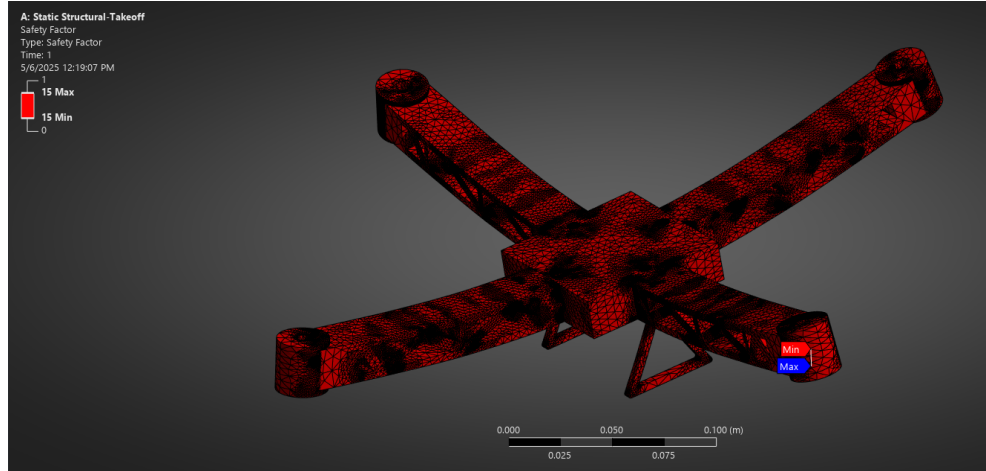


Figure 9: Drone Takeoff Factor of Safety (FOS)

The factors of safety for both minimum and maximum are 15. This demonstrates that the drone frame has ample margin for safe operation during takeoff.

3.1. b. Case B: Landing Load

Landing Impact Load Calculation:

Drone drop height (Assumed), $h=0.3$ m

$$\begin{aligned} \text{Impact Velocity, } v &= \sqrt{2gh} \\ &= \sqrt{2 * 9.81 * 0.3} \\ &= 2.426 \text{ m/s} \end{aligned}$$

Drone stopping time (Assumed) = 0.5s

$$\text{Impact Force, } F = \frac{mv}{t} = 1.805 \text{ N}$$

$$\text{Per leg (2 leg): } F_{\text{per leg}} = \frac{1.805}{2} = 0.903 \text{ N}$$

Boundary Conditions for Landing:

Supports (Fixed Constraints):

- The top faces of all four motor mounts were fixed in this case. This simulates the condition immediately after ground contact during landing, where the upper frame is restrained due to inertial reaction while impact forces are transferred through the legs.

Applied Loads:

- A vertical upward force of 0.903 N per leg was applied to the bottom face of each landing leg, representing the reaction force from the ground due to landing impact.

Purpose of Setup:

- This setup captures the way ground impact force transfers upward through the landing legs into the drone body, allowing analysis of stress and deformation from a sudden stop after descent.

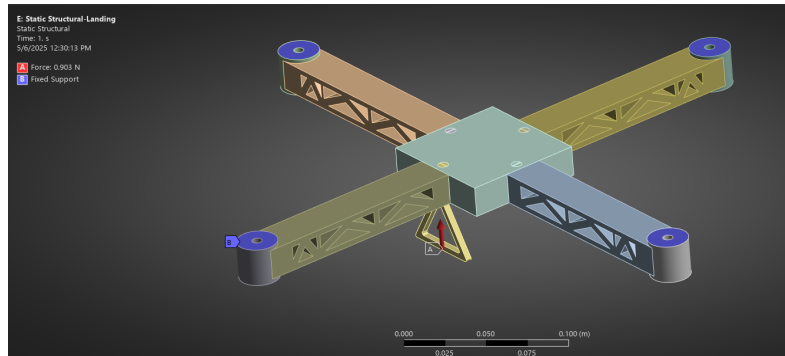


Figure 10: Landing Boundary Conditions

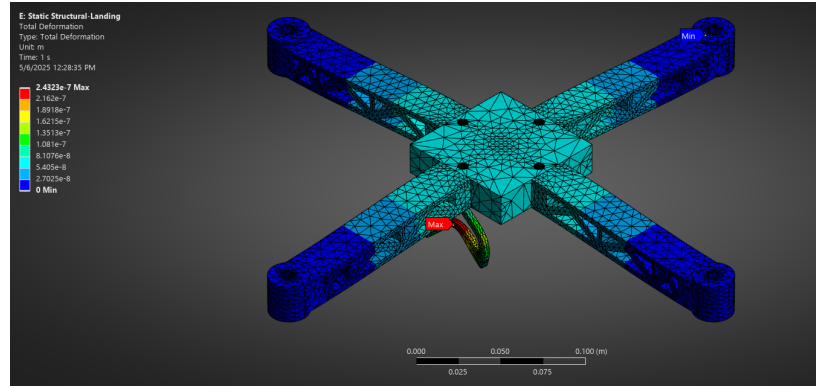


Figure 11: Landing Total Deformation

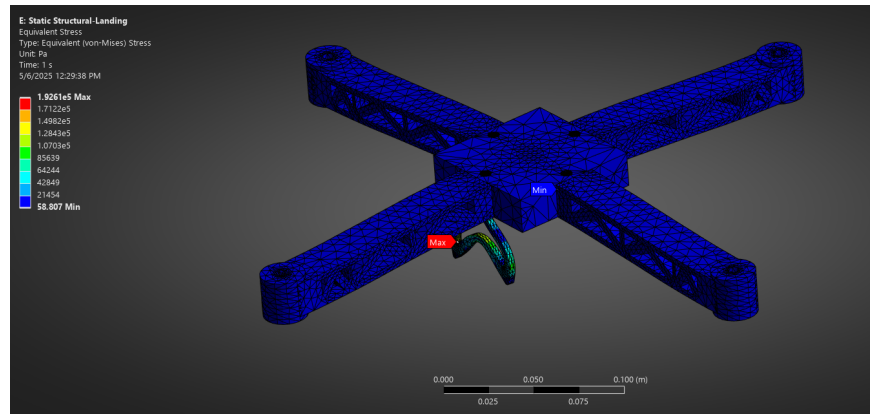


Figure 12: Equivalent (Von-Mises) Stress

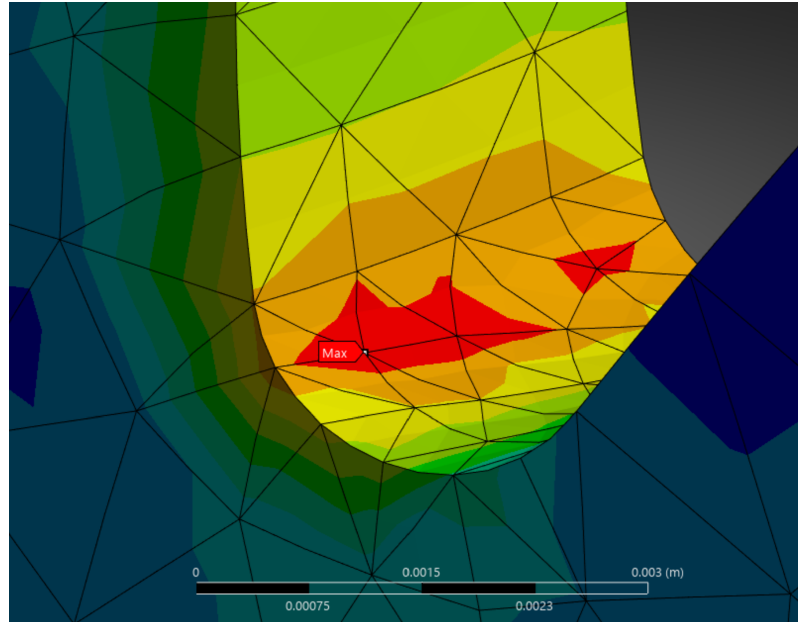


Figure 13: Close-Up View of Maximum Stress

Table 3: Average Stress for Landing

Time[s]	Minimum [Pa]	Maximum [Pa]	Average [Pa]
1.	58.807	1.9261E+005	8106

For the drone landing case, maximum stress was approximately 193 KPa, which is much lower than during takeoff. For this, the factor of safety is also analyzed in ANSYS. The factors of safety for both minimum and maximum are 15.

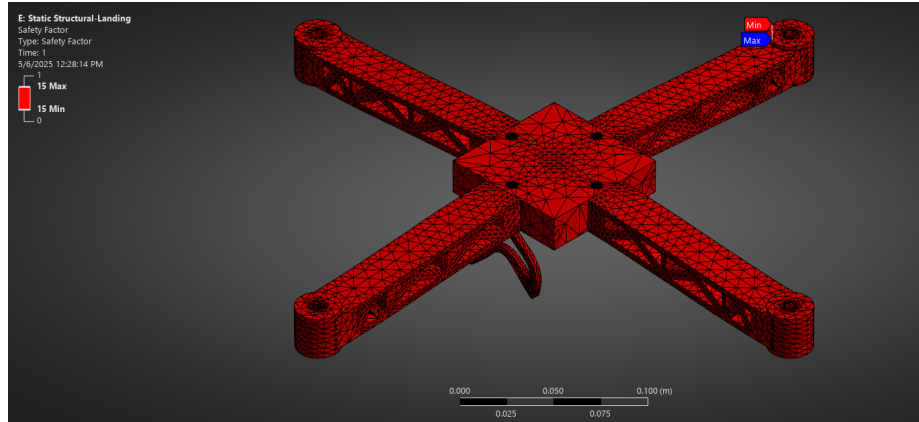


Figure 14: Drone Landing Factor of Safety

This demonstrates that even under impact conditions, the structure maintains the same high safety margin.

The static structural analysis under both takeoff and landing load conditions confirms that the drone frame, constructed from 6061-T6 Aluminum Alloy, is structurally sound and capable of withstanding real-world operational forces. Across both scenarios, the maximum equivalent (Von-Mises) stresses observed remain well below the material's tensile strength of 259 MPa, validating the material choice and structural configuration.

A safety factor of approximately 15 was observed in both takeoff and landing cases. This indicates that the drone frame can endure forces 15 times greater than the applied loads, demonstrating a high degree of structural robustness. Such a safety margin ensures an extremely low risk of failure, even in the presence of unforeseen impact forces, material defects, or manufacturing tolerances. While this suggests the design is highly conservative and potentially over-engineered, it is beneficial for prototype reliability and initial field testing.

The chosen fine mesh size of 0.02 mm enabled accurate stress resolution, particularly in critical regions such as the motor mounts and leg-to-frame junctions, where localized stress concentrations were expected and observed. These areas were monitored closely in both loading scenarios and remained safely within stress limits.

Overall, this analysis validates the feasibility, structural integrity, and reliability of the drone frame under key operational loads. The frame design ensures safe takeoff and landing, making it suitable for real-world deployment with confidence in its performance and durability.

3.2. Steady-State Thermal Analysis

The Steady-State Thermal analysis is used to understand and demonstrate the temperature distribution throughout the drone frame.

This analysis includes a set temperature for the body of the drone and two different convection rates that are applied to each face of the frame that experiences exposure to the surrounding air (Figure 15). The first convection was applied to the faces of the arms and legs, with a film coefficient of $15 \text{ W/m}^2\text{C}^\circ$. The second convection was applied to the propeller blades and pin surfaces, with a film coefficient of $137.5 \text{ W/m}^2\text{C}^\circ$. The film coefficient represents how effectively heat gets transferred between a solid surface and the air around it.

There are different film coefficients applied to the model because there is a difference between the airflow velocity and turbulence that each of those surfaces experiences. The propellers spin and generate high-speed airflow around them, thus increasing the *forced convection*, making the

coefficient fall between a range of 100-500. There is a higher airflow velocity, which creates a thinner boundary layer and a more efficient heat transfer. However, the arms and legs experience a lower airflow. They are more shielded by the surrounding components and are subjected to a *natural convection* that is created with a general drone motion.

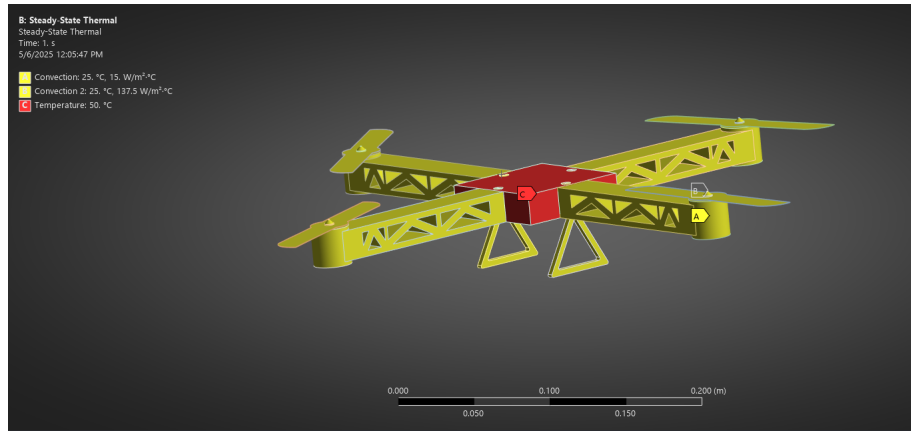


Figure 15: Boundary Conditions for Steady State Thermal Analysis

After applying the boundary conditions, the temperature distribution throughout the drone was analyzed (Figure 16). The body was set to a temperature of 50 degrees Celsius, so it remains at the same temperature throughout, which can be seen in the drone. The rest of the drone shows a distribution stemming from the body to the tip of the propellers, with a maximum of 50.035 degrees and a minimum of 25.223 degrees.

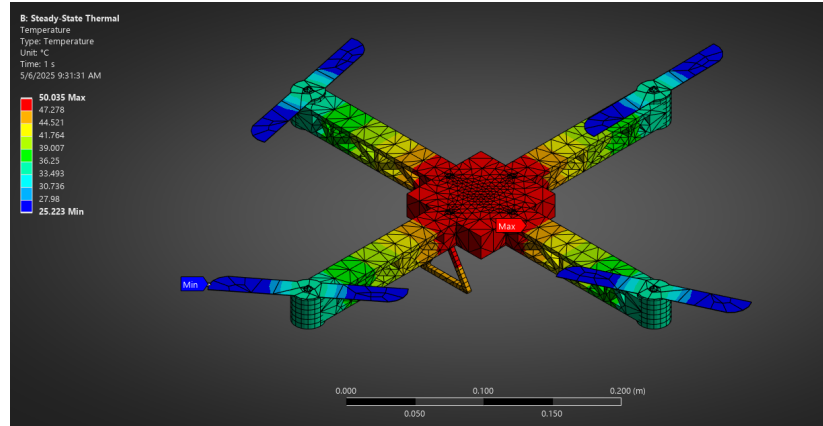


Figure 16: Thermal Temperature

The value of the total heat flux was analyzed to identify the hot spots and the cooling efficiency, and find where the heat is leaving or entering the different materials. Looking at the heat flow shows the direction the heat is flowing and identifies whether the heat is flowing toward sensitive electrons and away from them, whether the heat is being dissipated uniformly or unevenly, and how the design handles high temperatures. In the drone frame, Figure 17, it can be seen that the heat is distributed evenly throughout the body and the arms, and more unevenly in the propellers because the propellers have the most change in airflow, via convection.

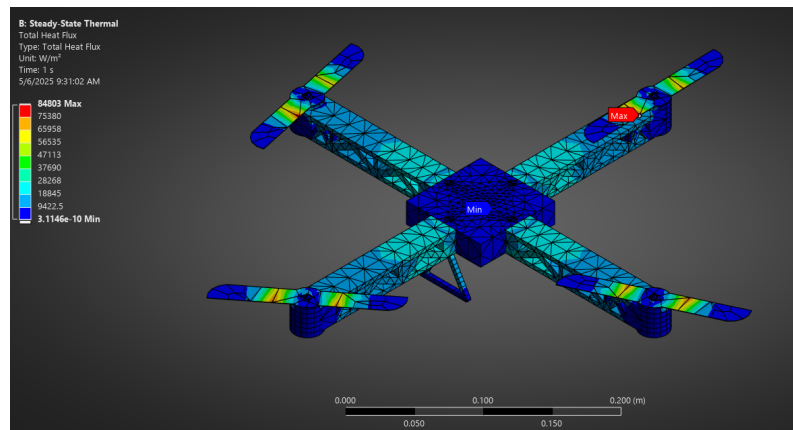


Figure 17: Thermal Total Heat Flux

The last thermal analysis was the thermal error, which typically refers to deformation and stress induced by temperature within the structure. This error is caused by non-uniform heating and thermal expansion, and for the drone frame, analyzing the thermal error tells how much the temperature has affected the mechanical integrity and functionality. The areas that had the most evident wear were in the blades nearest to the propeller pins and the cutouts within the arms of the drone (Figure 18). These areas are the most exposed to deformation and stress because of frame bending, twisting, and misalignments. However, most of the analyzed drone frames show a minimum value of 9.33×10^{-28} in error. This significantly low value of error shows the material is properly suited for the temperature environment, and the different parts handle internal stress well when under loads and increasing temperatures.

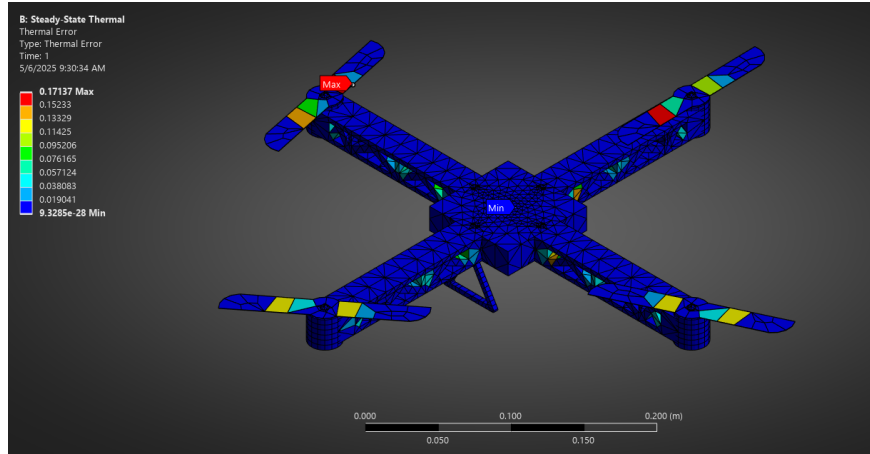


Figure 18: Thermal Error

Thermal analysis of the drone frame is done to determine how temperature affects the structural reliability. By applying these realistic conditions, it has become possible to identify inconsistencies and errors in the temperature distributions. It also helps with finding design issues that might lead to thermal stress and deformations. Understanding how the heat flux and

thermal errors run with the frame allows for design changes to keep it sound and functionally accurate under temperature conditions for flight, longevity, and performance.

3.3. Modal Analysis

Modal Analysis is used to understand how structures and objects vibrate as well as their resistance to applied forces. This analysis involves looking at natural frequencies, mode shapes, and damping characteristics. Each object has natural frequencies based on mass and stiffness, and specific frequencies at which the structure or object naturally vibrates when subjected to an external force or vibration. When the object vibrates at its natural frequency, resonance will occur, leading to large vibrations. The mode shape entails the specific patterns of vibration or deformation at each natural frequency. The shape of the model determines how different parts of the structure move relative to each other during vibration, which can include bending, twisting, etc. Damping involves measuring how vibration decays due to losing energy from friction or resistance over time, leading to a halt. The higher the damping, the faster vibrations will dissipate; this is crucial to measure to prevent excessive vibrations or minimize to avoid energy loss. This analysis can be applied to different industries: aerospace, automotive, musical instruments, etc. In aerospace, it is used to ensure components such as wings do not resonate at a high rate during flight to prevent fatigue or structural failure. Since our chosen model is a drone, these principles of Modal Analysis can be applied.

A Modal Analysis when the drone is at rest was run on SolidWorks to determine the natural frequencies, mode shapes, and damping characteristics. Boundary conditions applied to this analysis included two fixed faces on the bottom of the two legs of the drone to depict the drone fixed to the ground (Figure 19). The blades were suspended during this analysis to isolate and

accurately measure the structural dynamics of the drone frame without rotating components to prevent noise in the data, since modal analyses are linear, spinning blades create a non-linear effect, complicating analysis. By removing the blades, this ensures the focus of the analysis on the drone frame's response to external vibrations, which is crucial for identifying resonance, weak points, and damping.

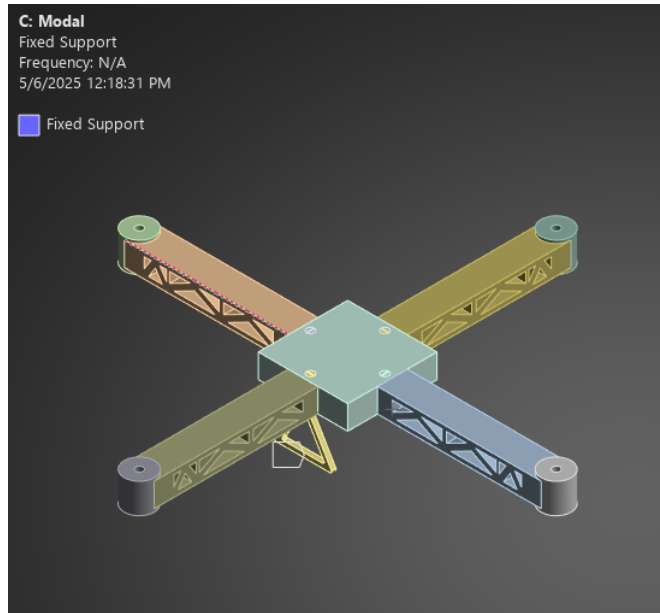


Figure 19: Modal Boundary Conditions

After defining the boundary conditions, 6-mode, or natural frequency, deformations were generated with a model shape. A choice of 6-mode results was made due to the first modes capturing critical vibration deformation patterns for drone modal analysis that can affect performance and safety. The first mode yielded a 50.8 Hz natural frequency with a maximum deformation of 2.570 m, with deformation concentrating on two arms across each other (Figure 20).

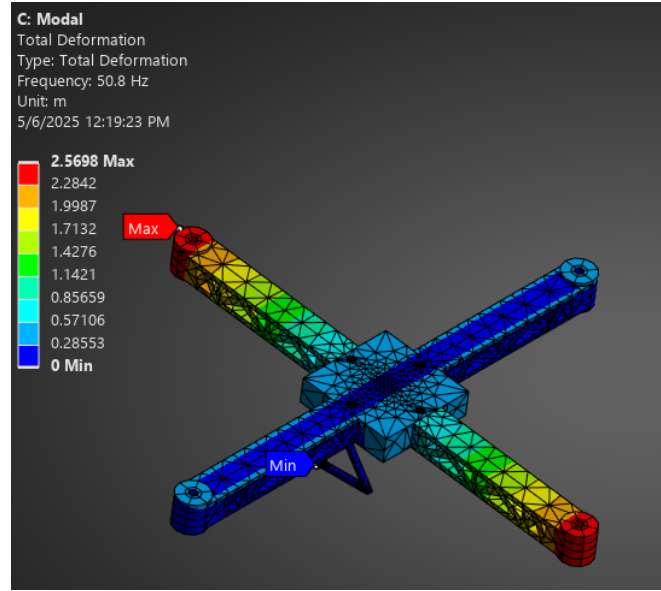


Figure 20: Total Deformation Mode 1

The second mode yielded a natural frequency of 120.38 Hz with a maximum deformation of 1.053 m concentration on the frame of the drone and bending of the legs (Figure 21).

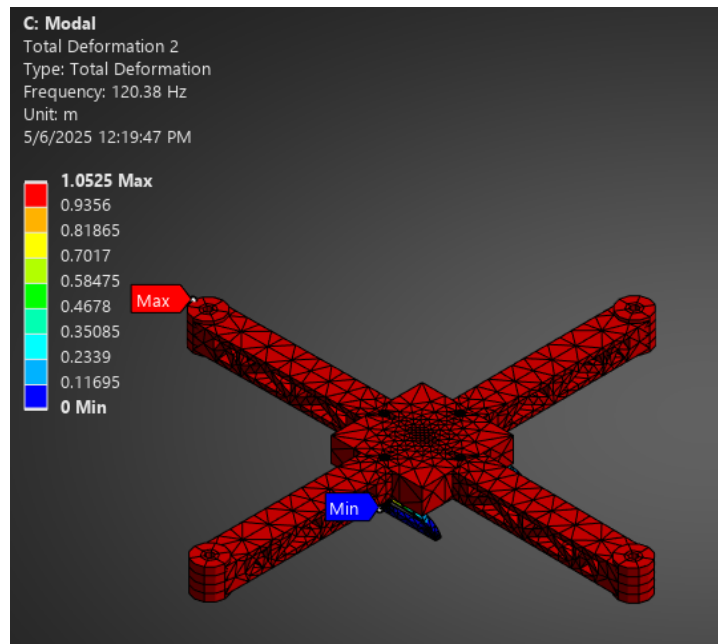


Figure 21: Total Deformation Mode 2

The third mode yielded a natural frequency of 244.51 Hz with maximum deformation of 1.897 m concentration on the end of all four arms (Figure 22).

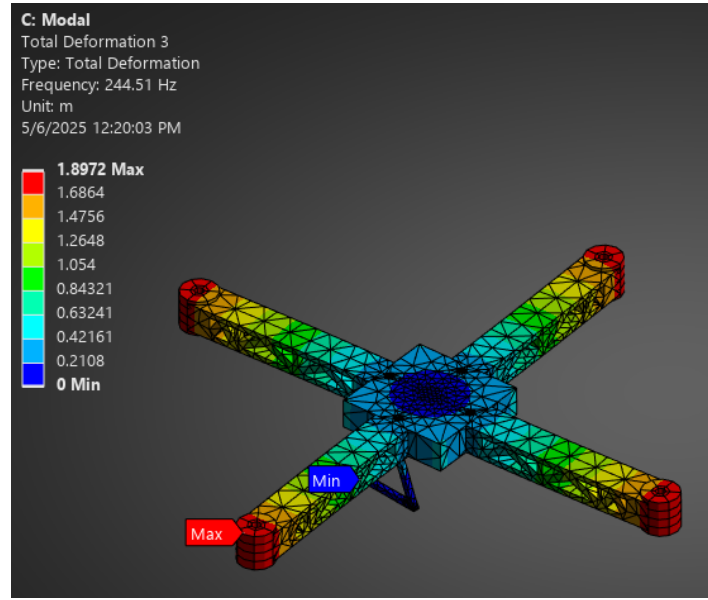


Figure 22: Total Deformation Mode 3

Mode 4 yielded a natural frequency of 441.91 Hz with a maximum deformation of 2.935 m, concentrating on two arms across each other (Figure 23).

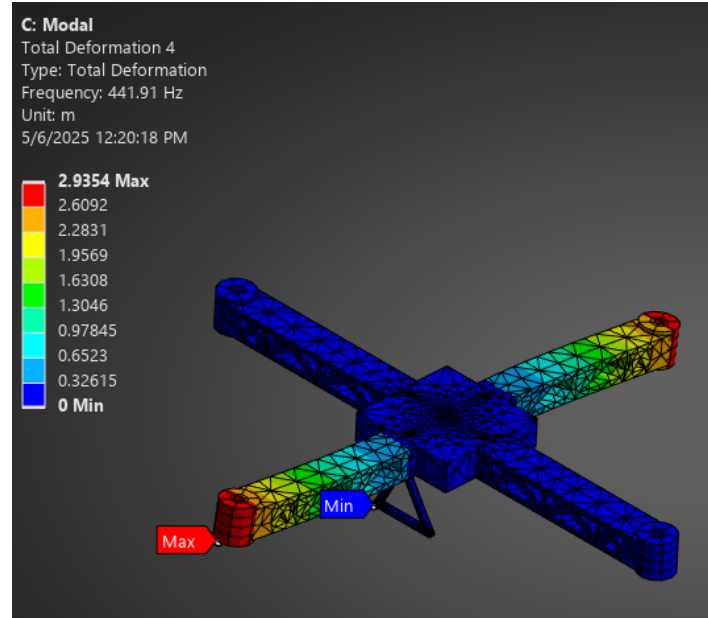


Figure 23: Total Deformation Mode 4

Mode 5 depicts a natural frequency of 529.06 Hz with a maximum deformation of 2.765 m, concentrating on the end of the arms bending upward (Figure 24).

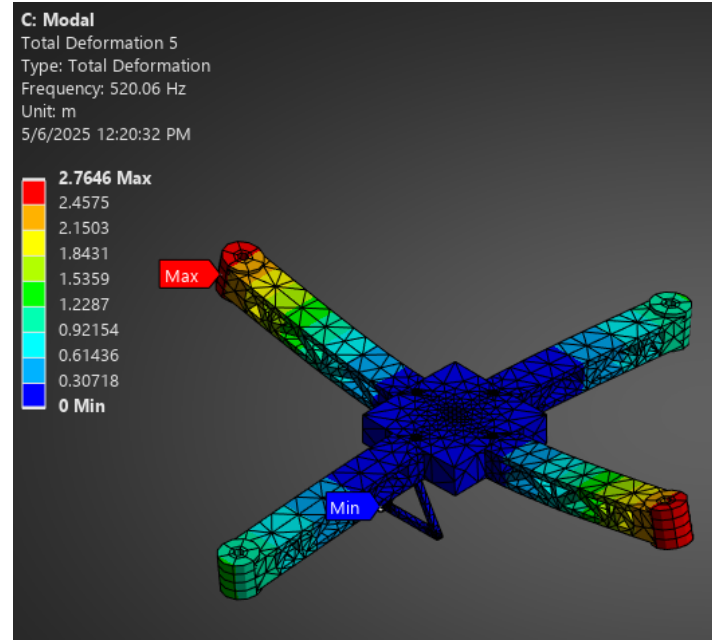


Figure 24: Total Deformation Mode 5

Lastly, mode 6 depicts a natural frequency of 559.98 Hz with a maximum deformation of 2.843 m concentrated on the end of the arms, where all arms are bending upward (Figure 25).

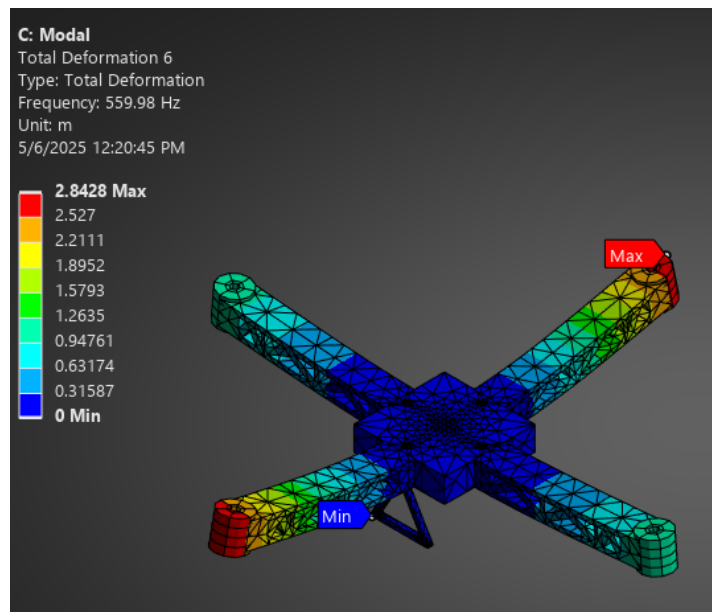


Figure 25: Total Deformation Mode 6

The natural frequencies of the drone frame depict a linear pattern (Figure 26), where each mode represents a higher natural frequency, indicating that the structure becomes progressively stiffer and resistant to deformation in higher modes. Mode 1 begins at 50.8 Hz and displays low-energy global bending, while mode 6 reaches 559.98 Hz to complex localized deformation. Lower modes capture large-scale motion and the higher modes reflect finer and stiffer behaviors, demonstrating good structural continuity and modal separation.

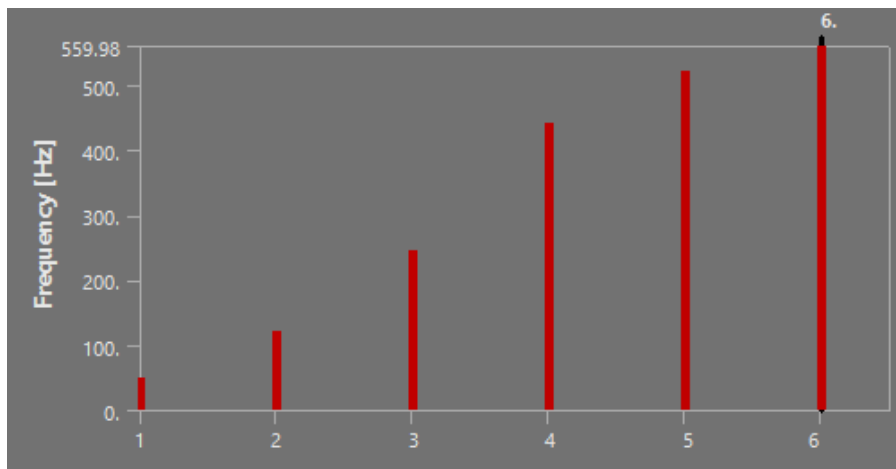


Figure 26: Total Deformation Mode 6

The motor speed is 1500 rad/s, and when converting that to Hz, we get 238.73 Hz. Only mode 3 was in range with that frequency, with 244.51 Hz. This indicates a high risk of resonance where the frame may experience amplified vibrations if excited near that natural frequency during flight, thus, the max of the model view is representative of the frame during that mode. Mode 3's natural frequency has a difference of 5.78 Hz, while the other mode's differences pass well over 100 Hz. This indicates that mode 3 falls directly in the operational range and poses a design concern where, without structural modification or added damping, the resonance could compromise flight stability, structural integrity, or long-term fatigue.

Table 4: Frequency of Modes

Mode	Frequency (Hz)	Difference
Comparison	238.73	-
1	50.8	187.93
2	120.38	118.35
3	244.51	5.78
4	441.91	203.18
5	520.06	281.33
6	559.98	321.25

3.4. Fluent Analysis

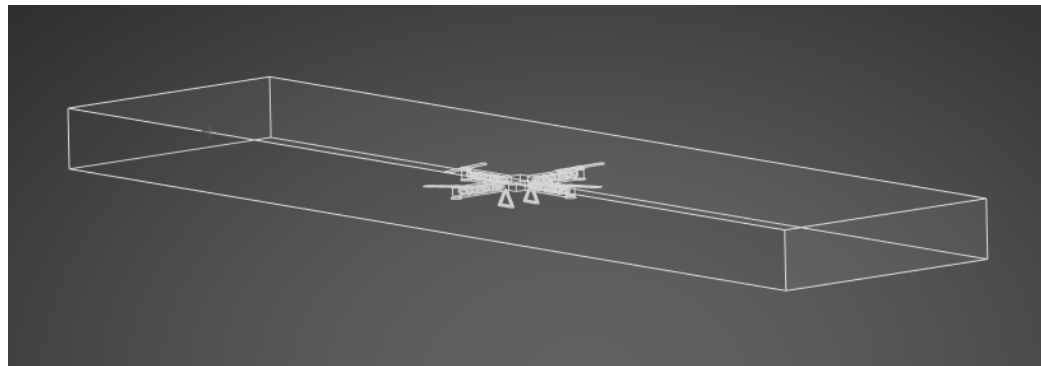


Figure 27: Enclosure Formed Around Drone for “Wind Tunnel”

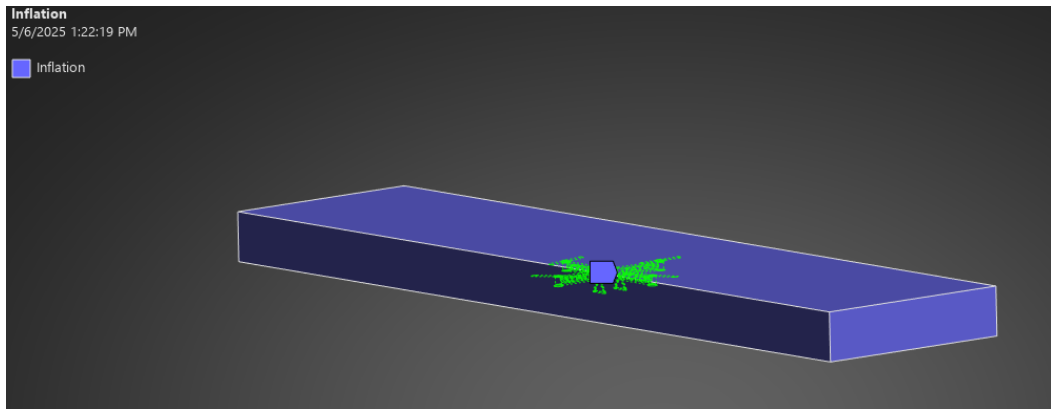


Figure 28: Inflation Mesh with Drone as Boundary Condition

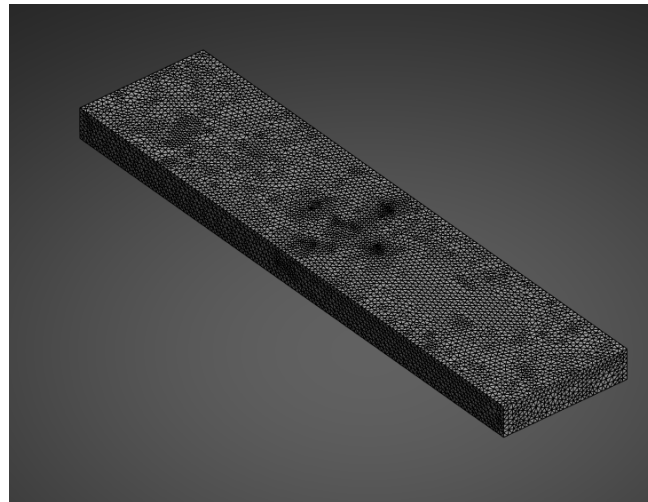
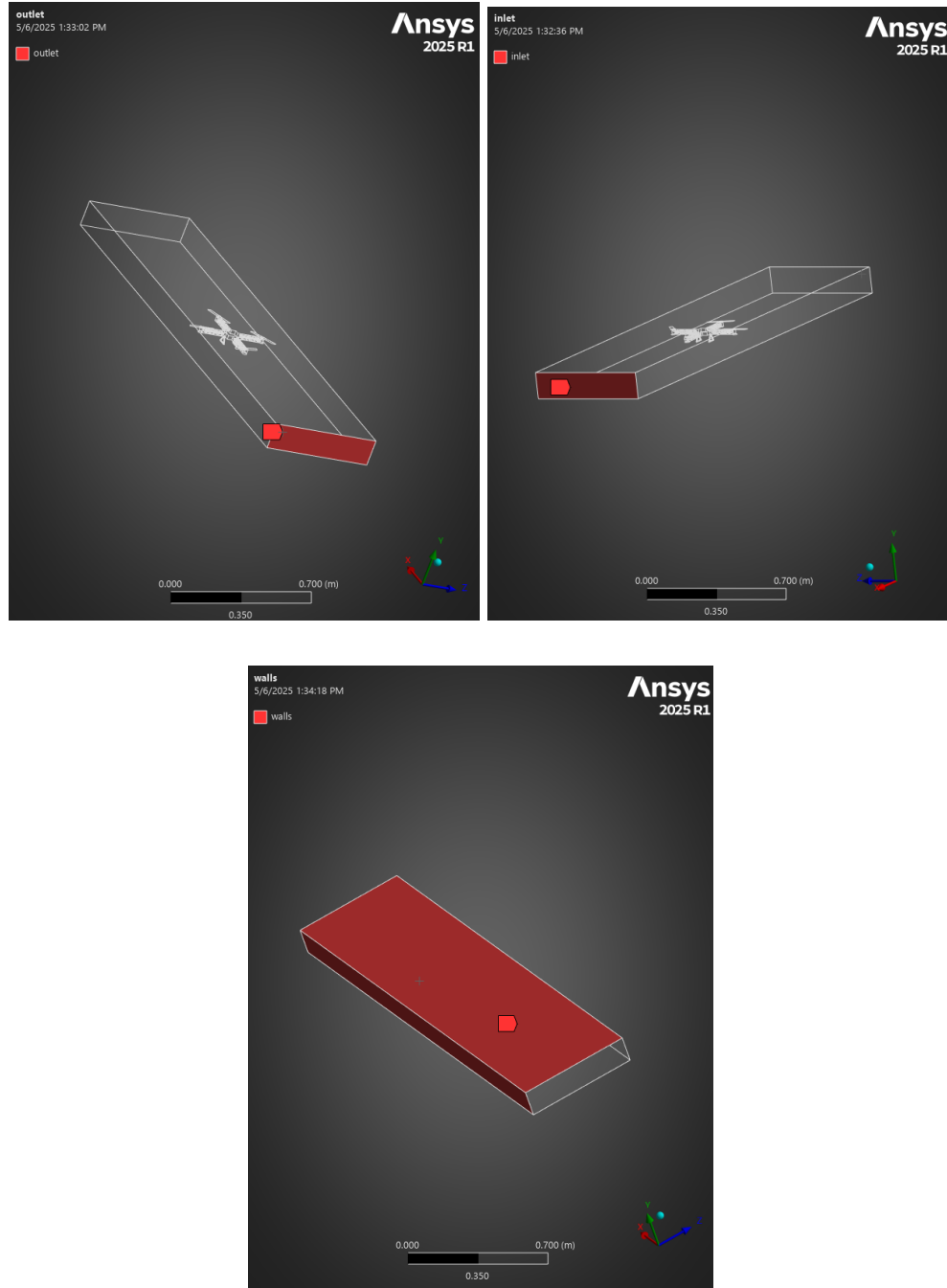


Figure 29: Mesh of Wind Tunnel

A wind tunnel was created in the fluent geometry, using the “Enclosure” tool in SpaceClaim. An Inflation mesh was then created as shown in the figures above, and named conditions of “inlet” and “outlet” were created to show the airflow within the wind tunnel, as shown in the figures below.



Figures 30, 31, & 32: Inlet, Outlet, and Walls Named Conditions

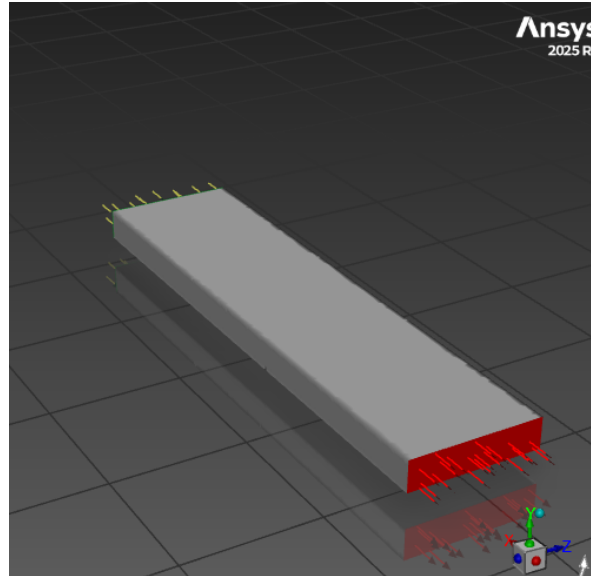


Figure 33: Velocity Inlet and Outlet

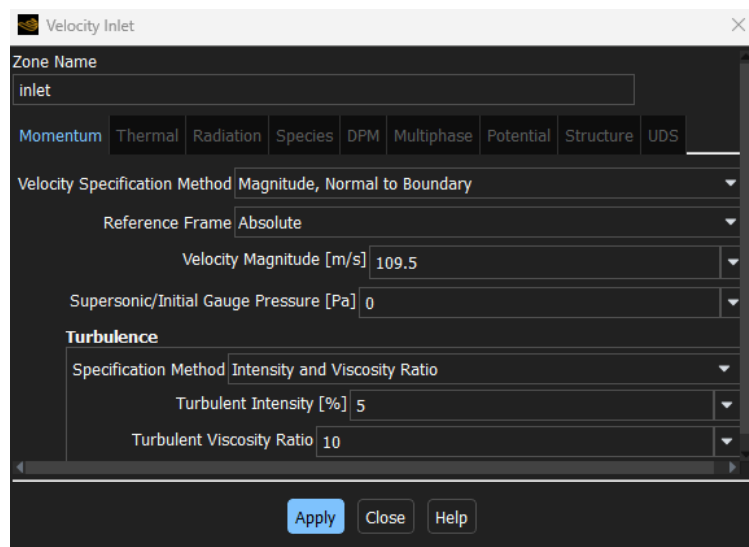


Figure 34: Inlet Velocity of 109.5 m/s

In Fluent, an inlet of velocity of 109.5 m/s was chosen. Since typical drone propellers range from 10,000 to 15,000 RPM. 1 RPM is about 9.5 rad/s, so after deciding the velocity of each propeller to be 1500 rad/s, which is 14,250 RPM, we can calculate the velocity of the drone.

$$\text{Propeller Radius: } 2.87'' = 0.072898 \text{ m}$$

$$\text{Velocity} = (0.072898)(1500) = 109.5 \text{ m/s}$$

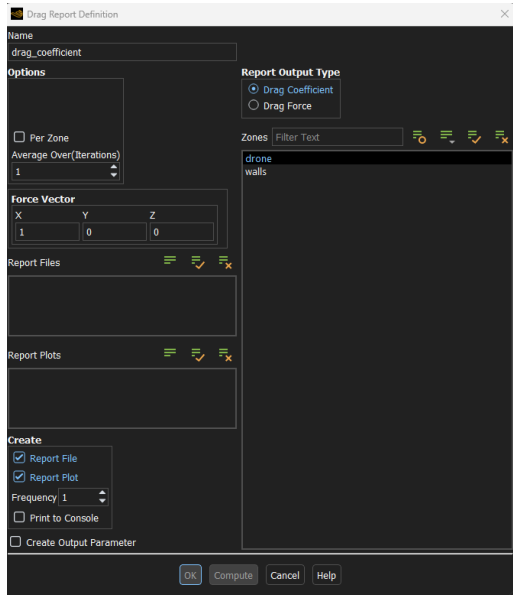


Figure 35: Drag Coefficient Report Definition

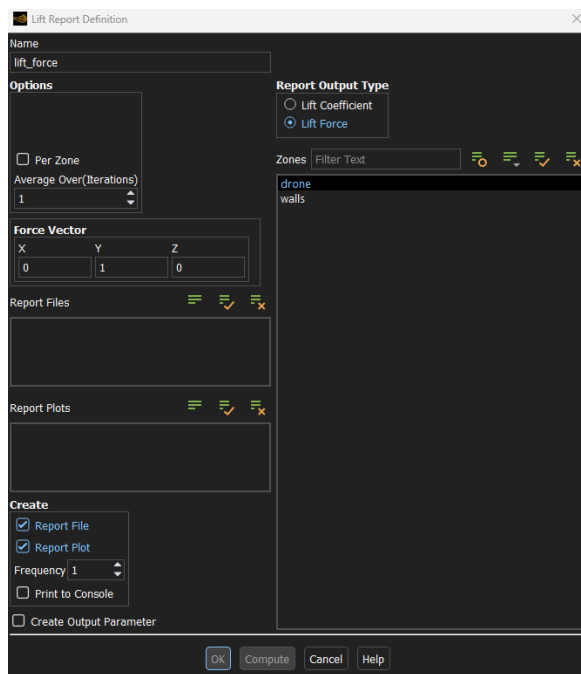


Figure 36: Lift Force Report Definition

In the figures above, the lift force and drag coefficient were chosen to be the results generated through fluent (CFD) analysis.

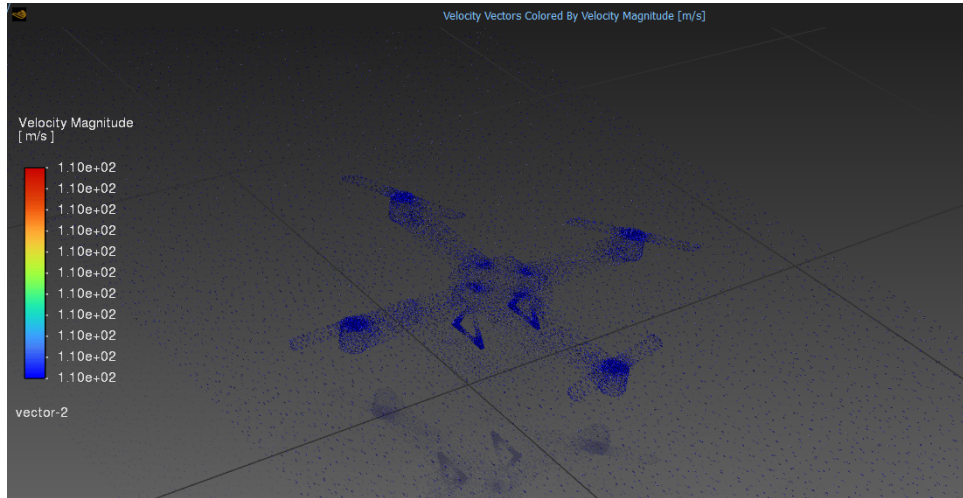
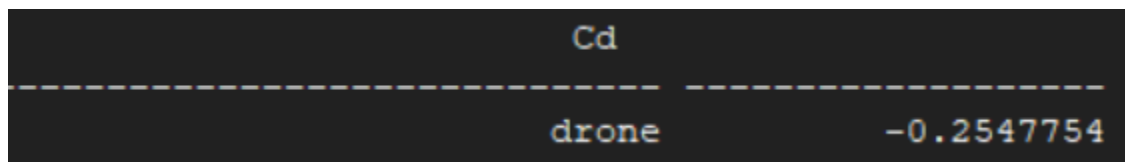
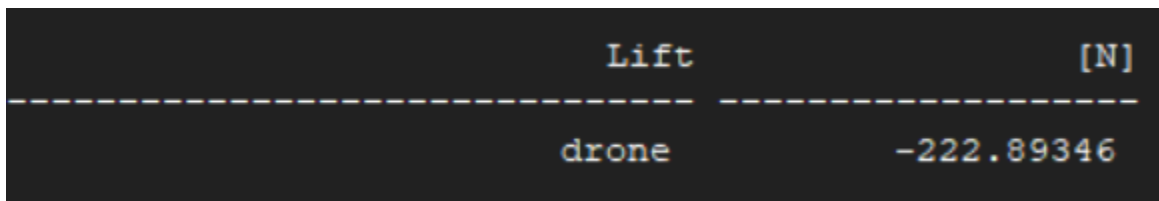


Figure 37: Velocity Magnitude



Figures 38 & 39: Lift Force and Drag Coefficient Result Values

The velocity magnitude was shown within the wind tunnel, consistently 109.5 m/s around the frame. The lift force in the drone was 222.89346 N, and the drone coefficient was 0.2547754.

```
/parallel/partition/use-stored-partitions

Migrating partitions to compute-nodes.

>> 8 Active Partitions:
```

P	Cells	I-Cells	Cell Ratio	Faces	I-Faces	Face Ratio	Neighbors	Load	Ext
Cells									
0	87532	884	0.010	197207	989	0.005	5	1	
899									
1	87637	4408	0.050	198796	5013	0.025	6	1	
4594									
2	86519	923	0.011	193010	1062	0.006	5	1	
993									
3	93867	898	0.010	195160	965	0.005	4	1	
898									
4	88070	1231	0.014	196863	1343	0.007	4	1	
1211									
5	88187	1022	0.012	196603	1109	0.006	5	1	
1022									
6	89533	1399	0.016	194739	1511	0.008	4	1	
1321									
7	89432	1478	0.017	194800	1608	0.008	3	1	
1398									
<hr/>									
Collective Partition Statistics:					Minimum	Maximum	Total		
<hr/>									
Cell count					86519	93867	710777		
Mean cell count deviation					-2.6%	5.7%			
Partition boundary cell count					884	4408	12243		
Partition boundary cell count ratio					1.0%	5.0%	1.7%		
<hr/>									
Face count					193010	198796	1560378		
Mean face count deviation					-1.5%	1.5%			
Partition boundary face count					965	5013	6800		
Partition boundary face count ratio					0.5%	2.5%	0.4%		

Partition neighbor count	3	6
<hr/>		
Partition Method	Metis	
Stored Partition Count	8	
Done.		

Figure 40: Stored Partition Results in Fluent Command Window

In the fluent analysis command window, the partition method was required to be chosen in order to run the drag and lift force program. The command /parallel/partition/use-stored-partitions was used to use the node elements from the generated inflation mesh in the fluent program, and the partition results shown in the figure above were developed.

The fluent analysis of the drone frame provided valuable insight into its aerodynamic performance. The simulation yielded a total lift force of 222.89346 N, which significantly exceeds the weight of the drone, indicating that there was more than sufficient lifting force. The large margin of lift ensures that the drone can hover and carry additional payloads. This can also prove that the drone can perform more aggressive maneuvers if necessary. The drag coefficient was calculated to be 0.2547754, which is considered low for the drone. This low value suggests that the frame design promotes good airflow, especially with the evidence of the well distributed velocity. The symmetry of the quadcopter supports balanced lift distribution across all four arms. The frame is both efficient and effective in handling airflow.

4. Discussion

The results obtained from the simulation studies provide a strong foundation for evaluating the drone frame's performance under real-world conditions. The primary objective was to verify

whether the frame could withstand physical stresses and thermal loads while maintaining structural stability and balance. The frame was subjected to both takeoff and landing forces during static structural analysis, and in both scenarios, the maximum stress values remained far below the yield strength of the chosen aluminum alloy. This suggests the structure can handle operational demands without compromising material integrity. Additionally, the uniform distribution of stress and low deformation observed in high-risk regions like motor mounts and leg junctions aligns with the design requirement for a balanced, durable frame.

One unexpected insight emerged during the modal analysis. While the frame exhibited increasing natural frequencies across the six modes, which is typical of well-behaved structural systems, the third mode, at 244.51 Hz, closely matched the motor excitation frequency of approximately 238.73 Hz. This near-alignment presents a potential risk of resonance, which was not initially anticipated, given that the analysis excluded the blades. However, this highlights a critical consideration where even without the rotating components modeled, the vibrations introduced through the motor mounts can still excite the frame. This mode-specific risk may not compromise overall functionality but could impact long-term durability and vibration-sensitive onboard components. Although the other modes are sufficiently separated from operational frequencies, the presence of this isolated resonance risk suggests that future design improvements should consider geometric or material adjustments to shift this mode further away from the operational range or integrate damping to reduce amplitude buildup.

Thermal analysis yielded predictable and stable results. The heat flow across the structure aligned well with expectations based on convection differences across components, and the

drone body maintained thermal stability with minimal variation. The propeller blades, which experienced the greatest heat flux variation, remained structurally unaffected, indicating strong thermal resilience. No thermal distortions or material compatibility issues were observed, reinforcing the appropriateness of the selected alloy for environments involving temperature exposure.

Fluent analysis predicted low drag and high lift values, indicating more than sufficient lifting capability for stable flight and maneuverability. With a high lift of around 222 N and a log drag coefficient of around 0.26, the drone frame demonstrates strong aerodynamic performance. The symmetrical quadcopter design promotes even airflow over the structure, reducing turbulence and enabling precise control in various flight conditions. The drone is proven to be well-optimized for both performance and energy conservation.

The simulation results of structural, thermal, modal, and fluent analyses confirm that the drone frame meets the initial design criteria of structural stability, thermal reliability, and vibration resistance under operating conditions. While the majority of the results aligned with expectations, the discovery of a mode with potential resonance during the modal analysis highlighted a critical exception. This emphasizes the value of incorporating multiple types of simulations to capture complex structural behaviors.

5. Conclusion

Through the application of finite element methods, our team confirmed that the drone frame meets the necessary requirements for structural integrity, thermal reliability, and aerodynamic stability. Each analysis supported that the frame can endure operational stresses, temperature variations, and vibrations without compromising performance or safety. The structural design remained well below material limits during takeoff and landing simulations, and the thermal and modal responses showed that the frame can maintain stability under realistic conditions. CFD results also indicated a favorable aerodynamic profile with efficient airflow and minimal drag.

As a group, we believe this drone frame design provides a strong foundation for real-world use. The consistent results across all analyses give us confidence in its reliability and durability. Moving forward, minor refinements, such as optimizing damping and further reducing drag, could improve performance, but the current frame demonstrates a well-balanced, functional, and safe design suitable for flight applications.

6. Appendix

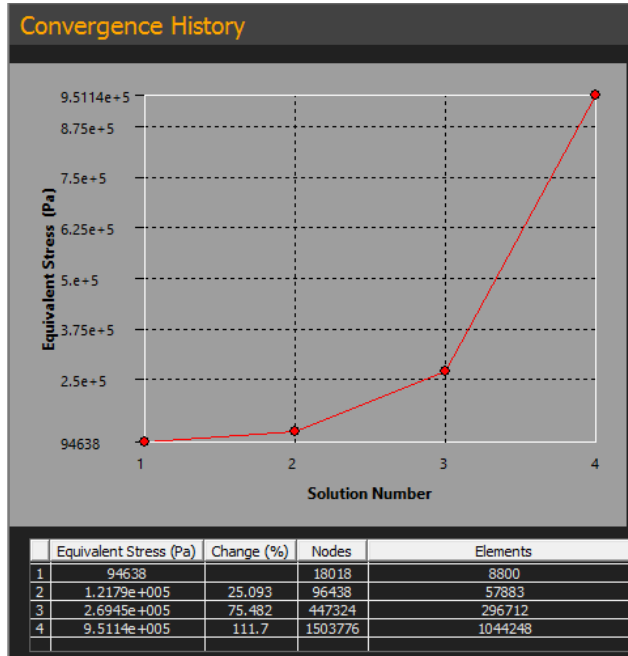


Figure 41: Takeoff Convergence Data

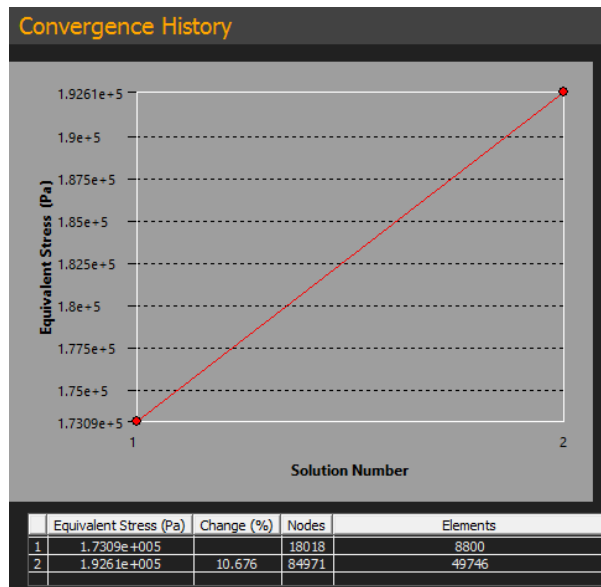


Figure 42: Drone Landing Convergence

7. References

1. ‘*Structural Analysis of Quadcopter Frame,*’ Singh/Kumar/Mishra/Agarwal,
<https://www.sciencedirect.com/science/article/pii/S2214785320320757>, accessed 4 May 2025.
2. “How to Choose the Right Motors and Propeller for Different Drone Applications?”
Grepow,
www.grepow.com/blog/how-to-choose-right-motors-and-propeller-for-different-drone-applications.html. Accessed 6 May 2025.
3. (PDF) *Modeling and Analysis of Quadcopter F450 Frame*,
www.researchgate.net/publication/340971107_Modeling_and_Analysis_of_Quadcopter_F450_Frame. Accessed 6 May 2025.